Nanoscale Research Letters
a SpringerOpen Journal

NANO IDEA   **Open Access**

Mo doping-enhanced dye absorption of Bi$_2$Se$_3$ nanoflowers

Mianzeng Zhong, Xiuqing Meng[*], Fengmin Wu, Jingbo Li[*] and Yunzhang Fang

Abstract

A simple solvothermal approach is explored to prepare Bi$_{2-x}$Mo$_x$Se$_3$ nanostructures by employing *N,N*-dimethylformamide (DMF) as the solvent. Mo plays an important role in the assembly of the Bi$_{2-x}$Mo$_x$Se$_3$ nanostructures from nanoplates to nanoflowers. Structural and morphological studies indicate that the resulting products are large specific surface area single-crystalline Bi$_{2-x}$Mo$_x$Se$_3$ nanoflowers self-assembled from thin nanoplates during the reaction process. The absorption properties of the as-prepared samples are investigated with Rhodamine B (RhB) as dye, and it is found that the Bi$_{1.85}$Mo$_{0.15}$Se$_3$ nanoflowers show an optimal adsorption capacity, implying that Mo doping not only changes the morphologies of the nanostructures but also enhances their absorption behaviors.

Keywords: Solvothermal; Bi$_{2-x}$Mo$_x$Se$_3$; Nanoflowers; Nanoplates; Higher adsorption capacity

Background

Water pollution has now become an urgent problem owing to the rapidly growing global industrial process [1,2]. Public health and social economies are threatened by various organic dye pollutants from textile industries [3]. A variety of methods have been introduced to remove dyes from wastewaters, such as membrane filtration [4], flotation [5,6], solvent extraction [7], chemical oxidation [8,9], adsorption [10,11], and photocatalytic degradation [12,13]. Among these methods, adsorption has been proved to be an effective way for wastewater treatment in terms of simplicity of design, user-friendly control, and insensitivity to toxic substances. Dye removal from industrial wastewaters by adsorption techniques has been widely concerned and researched in recent years [10-15]. Activated carbon is considered one of the best adsorbents for the removal of organic contaminants, but activated carbon is too expensive to use widely in practical applications [16]. Therefore, the development of low-cost, high-efficiency, renewable, and eco-friendly materials as absorbent for the removal of dyes has attracted more and more interests. Recently, many kinds of materials such as SnS$_2$ nanosheets [15], WO$_3$ nanorods [17], Cu$_2$O nanocrystals [18,19], and other highly adsorbent materials have been investigated.

Bismuth selenide (Bi$_2$Se$_3$) nanostructures have been extensively studied due to their unique properties and promising applications in the fields of optical recording systems, laser materials, optical filters, sensors, solar cells, strain gauges, electromechanical and thermoelectric devices, and topological insulators [20-23]. During the past few years, the preparation and application of doped Bi$_2$Se$_3$ have been extensively investigated [24-27]. In addition, due to the high surface state and unique optical or electrical properties [28], Bi$_2$Se$_3$ can also be applied in the fields of visible-light photocatalytic degradation [27,29]. For example, Bi$_2$Se$_3$-TiO$_2$ complex nanobelts [30] and S-doped BiSe [31] show excellent visible-light photocatalytic degradation performance. However, to our knowledge, there is no report on the absorption properties of Bi$_2$Se$_3$ nanostructures, especially the systematic study of the Mo doping-enhanced absorption behavior of Bi$_2$Se$_3$ nanostructures.

In this work, we synthesized self-assembled Mo-doped Bi$_2$Se$_3$ nanoflowers by a simple solvothermal route. We find that the absorption behavior of Bi$_{2-x}$Mo$_x$Se$_3$ on Rhodamine B (RhB) varies as a function of Mo content and reaches its highest absorption capacity with 15% Mo doping.

Methods

Preparation of Bi$_{2-x}$Mo$_x$Se$_3$

All of the chemical reagents used in this experiment are of analytical grade and used without further purification.

* Correspondence: xqmeng@semi.ac.cn; jbli@semi.ac.cn
Research Center for Light Emitting Diodes (LED), Zhejiang Normal University, Jinhua, Zhejiang Province 321004, China
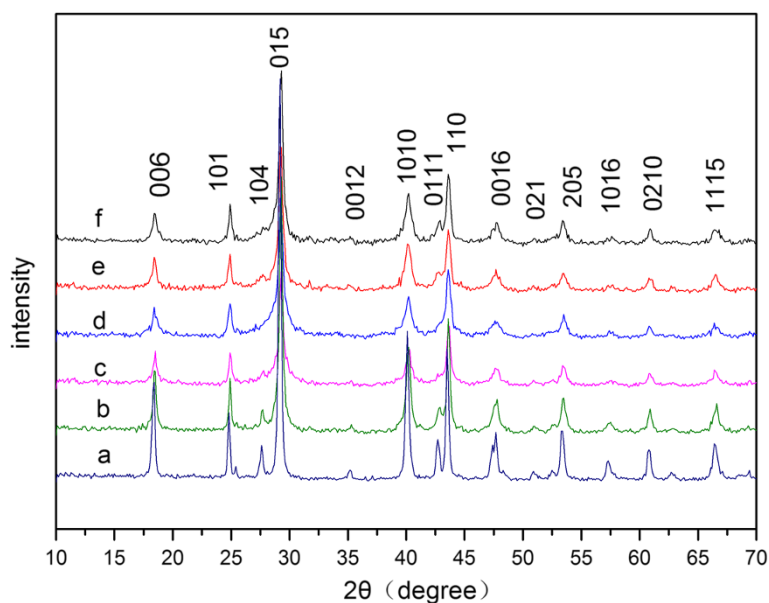
Figure 1 XRD patterns of samples (a) A, (b) B, (c) C, (d) D, (e) E, and (f) F.

$Bi_{2-x}Mo_xSe_3$ (x = 0, 0.01, 0.03, 0.05, 0.10, and 0.15) is obtained by a simple solvothermal method. In a typical $Bi_{2-x}Mo_xSe_3$ (x = 0.15) synthesis, 0.85 mmol of Bi $(NO_3)_3 \cdot 5H_2O$ and 0.15 mmol of $(NH_4)_6Mo_7O_{24} \cdot 4H_2O$ are added to 18 ml of N,N-dimethylformamide under vigorous stirring to form a homogeneous solution. Then additional ammonia is added to the above solution to adjust the pH value to 9 to 10 under continuous stirring. After that, Se powder and Na_2SO_3 are added to the above solution under magnetic stirring. The final solution is transferred into a Teflon-lined autoclave (25-ml capacity), kept at 160°C for 20 h, and cooled to room temperature under ambient conditions. The products are finally washed several times with ethanol and distilled water, followed by drying at 80°C for 12 h under vacuum. For comparison, we also synthesized $Bi_{2-x}Mo_xSe_3$ samples with different Mo contents (x = 0, 0.01, 0.03, 0.05, 0.10, and 0.15), which are labeled as samples A, B, C, D, E, and F, respectively.

Dye adsorption experiments

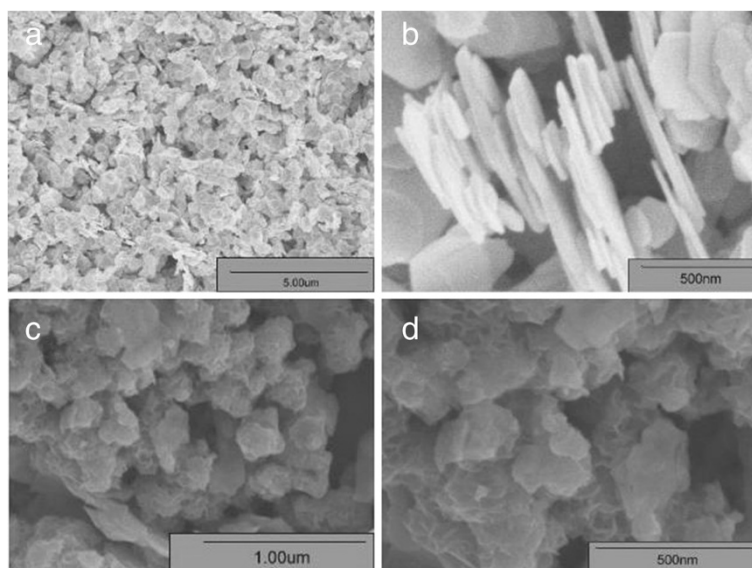The adsorption activities of the as-prepared products are investigated using RhB as dyes. In each experiment, 0.08 g

Figure 2 Low-resolution FESEM images of samples (a) A and (c) F and their respective high-resolution SEM images (b, d).
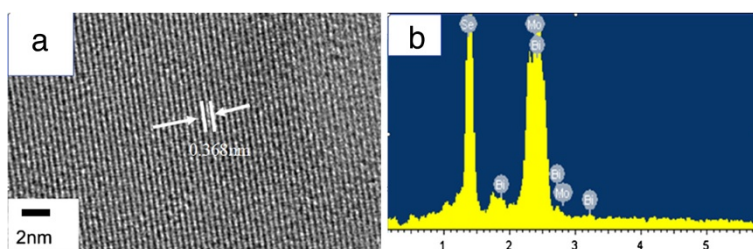
Figure 3 A HRTEM image of sample F (a) and the EDXA spectrum of sample F (b).

of adsorbent was added to 50 ml of a 10-mg/l RhB solution. Under constant stirring in the dark, about 6 ml of the mixture solution is taken out at intervals and centrifuged to separate solid particles for analysis. After centrifugation, the adsorption behavior is investigated.

Sample characterization

The phase composition and crystallographic structure of the as-prepared samples are examined by X-ray diffraction (XRD) technique with Cu Kα irradiation. The sizes and morphologies of the products are investigated using a field emission scanning electron microscope (FESEM; S-4800, Hitachi, Minato-ku, Tokyo, Japan). The dye adsorption behavior is measured with a UV-visible (UV–vis) spectrum (Lambda 900, PerkinElmer Instruments, Branford, CT, USA).

Results and discussion

Structure and morphology

The as-prepared samples are examined by XRD techniques, and the XRD patterns of samples A to F are shown in Figure 1. All the peaks in the patterns can be indexed according to the power diffraction card of hexagonal Bi_2Se_3 (no. 33-0214), and no impurity phase related to the Mo complex could be found. The diffraction peaks shift to higher angles with the increase of Mo^{6+} content from samples A to F, indicating that Mo^{6+} has been incorporated in the Bi_2Se_3 lattice, and the lattice parameter gets smaller with the increase of Mo^{6+}. This is understandable considering the fact that the ionic radius of Mo^{6+} (0.065 nm) [24] is smaller than that of Bi^{3+} (0.103 nm) [25].

The morphology and size of the as-synthesized products are characterized by FESEM observations (Figure 2). The low-magnification FESEM image in Figure 2a shows that a large number of platelike nanostructures are randomly dispersed on the surface of the substrate. Comparatively, a perfect hexagonal morphology for Bi_2Se_3 is observed from the image. A magnified FESEM image (Figure 2b) shows that the width of the nanosheets is in the range of 100 to 400 nm with a thickness of about 10 to 30 nm. The doping of Mo changes the morphologies of the nanosheets greatly. The low-magnified FESEM
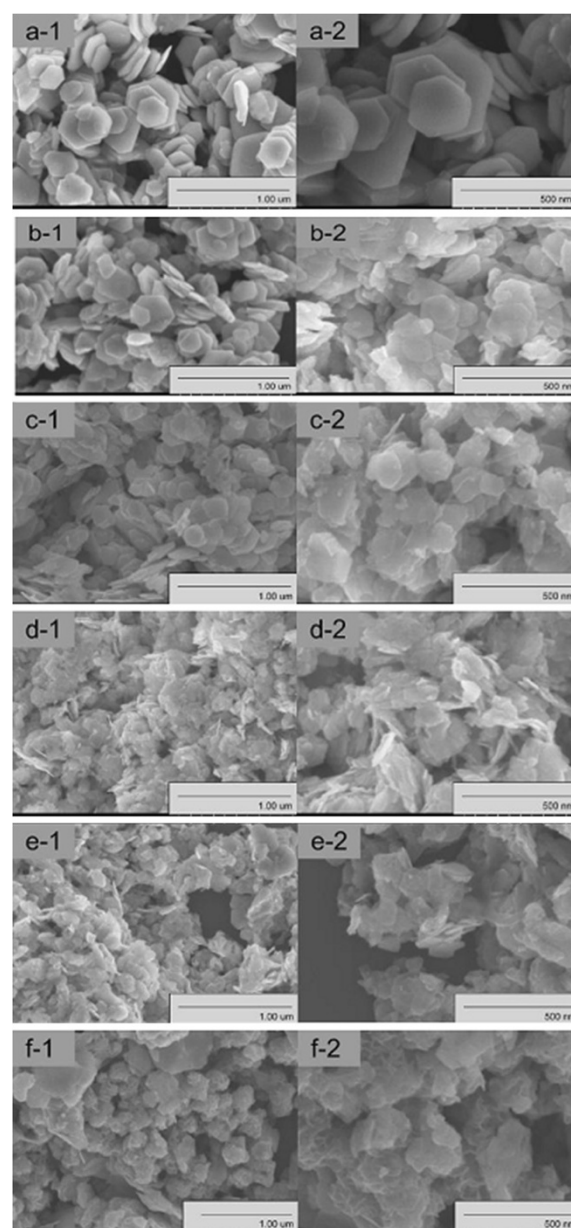

Figure 4 Low- and high-magnification FESEM images of the samples. Low-magnification **(a1, b1, c1, d1, e1, and f1)** and high-magnification **(a2, b2, c2, d2, e2, and f2)** FESEM images of samples A **(a1, a2)**, B **(b1, b2)**, C **(c1, c2)**, D **(d1, d2)**, E **(e1, e2)**, and F **(f1, f2)**.

image (Figure 2c) demonstrates that the typical product of $Bi_{1.85}Mo_{0.15}Se_3$ consists of a large quantity of uniform flowerlike nanospheres. The average diameter of flowerlike nanospheres is about 100 to 200 nm, and they are made up of curved nanoplates with an average thickness of 5 to 10 nm as shown in the high-magnification FESEM image (Figure 2d).

To confirm the structure, crystallinity, and details of the flowerlike nanospheres, high-resolution transmission electron microscopy (HRTEM) techniques are employed. A representative HRTEM image taken from the edge of a $Bi_{1.85}Mo_{0.15}Se_3$ nanoflower is shown in Figure 3a, which clearly indicates that nanoflowers contain a perfectly periodic arrangement with an interplanar distance of $a = 0.356$ nm, which is smaller than that of bulk anatase ($a = 0.413$ nm) crystal.

The chemical composition of $Bi_{2-x}Mo_xSe_3$ was determined by energy-dispersive X-ray analysis (EDXA) attached to the FESEM. In Figure 3b, the EDXA spectrum of the $Bi_{1.85}Mo_{0.15}Se_3$ nanosheets shows that the nanosheets contain only Mo, Bi, and Se without any trace of by-products.

From the FESEM observations, we can conclude that the Mo concentration influences the morphologies of the nanoplates greatly. In order to understand the role of Mo in the evolution process of $Bi_{2-x}Mo_xSe_3$ from nanoplates to nanoflowers, $Bi_{2-x}Mo_xSe_3$ samples with varied x values are synthesized and studied. With the increase of the x value (Mo concentration), the nanostructures gradually change from hexagonal nanosheets to smaller-sized hexagonal nanosheets and finally to flowerlike spheres, combined with a size change. For example, when no Mo is contained, the sizes of the nanosheet are about 100 to 500 nm in width and 20 to 30 nm in thickness, as shown in Figure 4 (a-1 and a-2). With increasing amounts of Mo, morphologies of the as-synthesized $Bi_{2-x}Mo_xSe_3$ products change from nanosheets to nanoflowers (Figure 4 (a-1 to f-2). From Figure 4 (b-1 to d-2), we can see that the products are still composed of nanosheets, but the sizes of Bi_2Se_3 have become smaller. When the Mo concentration increased up to 15% (Figure 4 (f-1 and f-2), regular

flowerlike spheres consisting of thin nanoplates were formed. The average diameter of nanoflowers is about 100 to 200 nm, and they are made up of curved nanoplates with an average thickness of 5 to 10 nm as shown in the magnified image. With the increase of Mo contents in $Bi_{2-x}Mo_xSe_3$, the diameter of the products was found to be lower than that of pure Bi_2Se_3. So we believe that Mo is the main driving force for the formation of a flowerlike structure.

A diagram of the formation mechanism of nanoplates and nanoflowers of $Bi_{2-x}Mo_xSe_3$ is presented in Figure 5. When no Mo is contained, tiny clusters of Bi_2Se_3 nanosheets are first generated upon heating and then enriched to assemble into bigger nanosheets. However, with the increase of Mo concentration in $Bi_{2-x}Mo_xSe_3$, nanosheets assemble into nanoflowers.

Adsorption ability of $Bi_{2-x}Mo_xSe_3$

To investigate the potential application of the as-synthesized $Bi_{2-x}Mo_xSe_3$ nanocrystals and their relationship with the amount of Mo in $Bi_{2-x}Mo_xSe_3$, we study the adsorption ability of $Bi_{2-x}Mo_xSe_3$ using RhB as dyes. The experiments are carried out with $Bi_{2-x}Mo_xSe_3$ dispersed in the solution of RhB in the dark several times with constant stirring. After centrifugation, the UV–vis absorption of the supernatant was measured and the characteristic absorption of RhB at about 553 nm was selected to estimate the adsorption process. Figure 6 shows the UV–vis adsorption spectra of RhB as a function of time using the as-prepared $Bi_{1.99}Mo_{0.01}Se_3$ as adsorbent. From Figure 6, we can see that the intensity of the absorption spectra gradually decreases and nearly disappears within 60 min; at the same time, the solution becomes colorless when observed with the naked eye.

Figure 7 shows the variation in RhB concentration with the adsorption time over different adsorbents. When there is no adsorbent, the concentration of the RhB solution remains the same with its original state for up to 60 min, which demonstrates that RhB is stable under the experimental conditions. Pure Bi_2Se_3 shows a weak adsorption
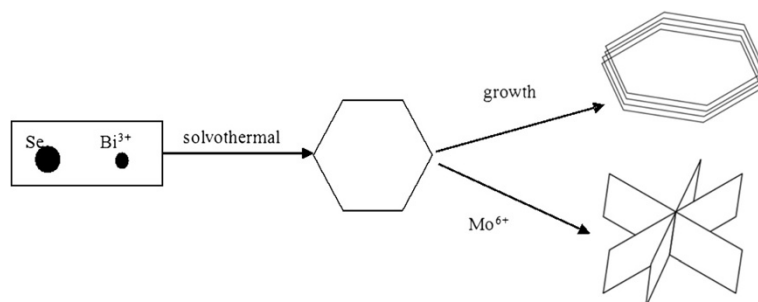

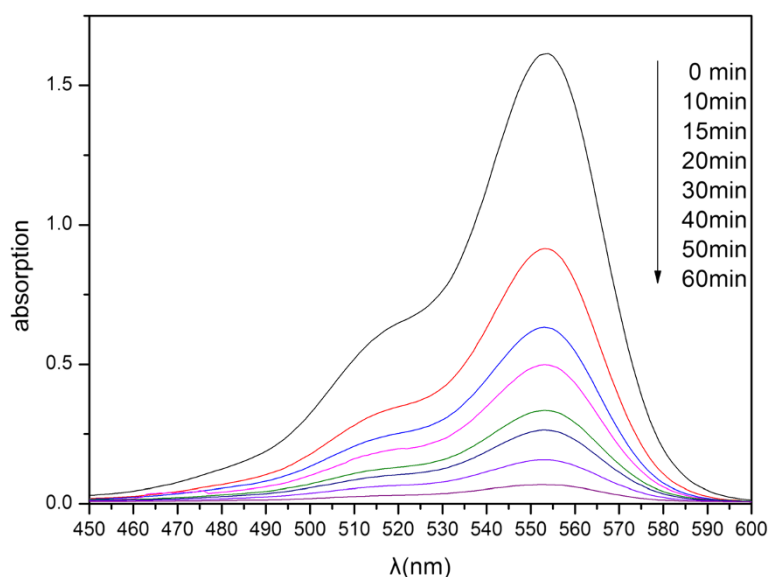**Figure 5 Schematic diagram showing the growth mechanism of nanosheets and nanoflowers of $Bi_{2-x}Mo_xSe_3$.**

Figure 6 Time-dependent absorption of 2.0×10^{-4} M 50-ml aqueous solutions of RhB in the presence of 50-mg as-prepared $Bi_{1.99}Mo_{0.01}Se_3$.

activity. After 60 min of absorption, only 20% of RhB is removed from the pure Bi_2Se_3 sample. The adsorption activities are strengthened with the increase of Mo contents in Bi_2Se_3. $Bi_{1.85}Mo_{0.15}Se_3$ has a maximum adsorption behavior, and nearly 100% of the RhB dyes are removed in 20 min. All of this clearly shows that the doping of Mo in Bi_2Se_3 is an efficient way to enhance its adsorption activity. The results indicate that the as-synthesized $Bi_{2-x}Mo_xSe_3$ might possess a profound application in the fields of treatment of dye-polluted wastewater.

Conclusions

In summary, $Bi_{2-x}Mo_xSe_3$ nanomaterials were prepared by a solvothermal approach, and different morphologies of $Bi_{2-x}Mo_xSe_3$ have been obtained. The doping concentration of Mo plays an important role in controlling both the morphologies of $Bi_{2-x}Mo_xSe_3$ nanostructures and their absorption behavior. The sample with the best absorption behavior is that with 15% Mo concentration. We believe that the study of dye absorption behavior brings a new application realm for Bi_2Se_3 nanostructures.
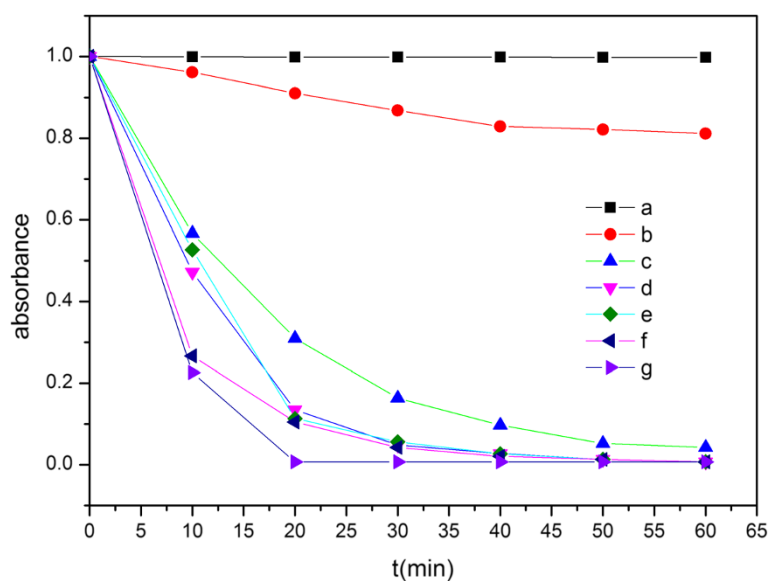

Figure 7 A plot showing the extent of RhB degradation as a function of adsorption time for different catalysts. RhB degradation is monitored at 554 nm. Lines **a, b, c, d, e, f,** and **g** represent, respectively, samples blank, A, B, C, D, E, and F.

References
1. Schwarzenbach RP, Egli T, Hofstetter TB, von Gunten U, Wehrli B: **Global water pollution and human health.** *Annu Rev Environ Resour* 2010, **35**:109–136.
2. Hanley N, Shogren J, White B: *Introduction to Environmental Economics.* Oxford: Oxford University Press; 2013:1–20.
3. Laing IG: **The impact of effluent regulations on the dyeing industry.** *Rev Prog Color Relat Top* 1991, **21**(1):56–71.
4. Ersahin ME, Ozgun H, Dereli RK, Ozturk I, Roest K, van Lier JB: **A review on dynamic membrane filtration: materials, applications and future perspectives.** *Bioresour Technol* 2012, **122**:196–206.
5. Zodi S, Merzouk B, Potier O, Lapicque F, Leclerc JP: **Direct red 81 dye removal by a continuous flow electrocoagulation/flotation reactor.** *Sep Purif Technol* 2013, **108**:215–222.
6. Zheng YM, Yunus RF, Nanayakkara KGN, Chen JP: **Electrochemical decoloration of synthetic wastewater containing rhodamine 6G: behaviors and mechanism.** *Ind Eng Chem Res* 2012, **51**(17):5953–5960.
7. Hu HS, Yang MD, Dang J: **Treatment of strong acid dye wastewater by solvent extraction.** *Separation and Purification Technology* 2005, **42**(2):129–136.
8. Malik PK, Saha SK: **Oxidation of direct dyes with hydrogen peroxide using ferrous ion as catalyst.** *Sep Purif Technol* 2003, **31**(3):241–250.
9. Chen X, Xue Z, Yao Y, Wang W, Zhu F, Hong C: **Oxidation degradation of rhodamine B in aqueous by treatment system.** *Int J Photoenergy* 2012, **2012**:1–5.
10. Mittal A, Thakur V, Gajbe V: **Adsorptive removal of toxic azo dye Amido Black 10B by hen feather.** *Environ Sci Pollut Res* 2013, **20**(1):260–269.
11. Khan TA, Dahiya S, Ali I: **Use of kaolinite as adsorbent: equilibrium, dynamics and thermodynamic studies on the adsorption of rhodamine B from aqueous solution.** *Appl Clay Sci* 2012, **69**:58–66.
12. Turchi CS, Ollis DF: **Photocatalytic degradation of organic water contaminants: mechanisms involving hydroxyl radical attack.** *Journal of Catalysis* 1990, **122**(1):178–192.
13. Le HA, Linh LT, Chin S, Jurng J: **Photocatalytic degradation of methylene blue by a combination of TiO2-anatase and coconut shell activated carbon.** *Powder Technol* 2012, **225**:167–175.
14. Zhang W, Shi L, Tang K, Liu Z: **Synthesis, surface group modification of 3D MnV2O6 nanostructures and adsorption effect on Rhodamine B.** *Mater Res Bull* 2012, **47**(7):1725–1733.
15. Li X, Zhu J, Lv FJ, Wang JG, Xie ZL, Hoang M, Li HX: **An efficient removal of rhodamine B in water by targeted adsorption on SnS2 nanosheets.** *Adv Mater Res* 2012, **356**:1708–1711.
16. Mezohegyi G, van der Zee FP, Font J, Fortuny A, Fabregat A: **Towards advanced aqueous dye removal processes: a short review on the versatile role of activated carbon.** *J Environ Manage* 2012, **102**:148–164.
17. Zhu J, Wang S, Xie S, Li H: **Hexagonal single crystal growth of WO3 nanorods along a [110] axis with enhanced adsorption capacity.** *Chem Commun* 2011, **47**(15):4403–4405.
18. Li B, Cao H, Yin G, Lu Y, Yin J: **Cu2O@ reduced graphene oxide composite for removal of contaminants from water and supercapacitors.** *J Mater Chem* 2011, **21**(29):10645–10648.
19. Shang Y, Zhang D, Guo L: **CuCl-intermediated construction of short-range-ordered Cu2O mesoporous spheres with excellent adsorption performance.** *J Mater Chem* 2012, **22**(3):856–861.
20. Batabyal SK, Basu C, Das AR, Sanyal GS: **Solvothermal synthesis of bismuth selenide nanotubes.** *Mater Lett* 2006, **60**(21):2582–2585.
21. Cho S, Butch NP, Paglione J, Fuhrer MS: **Insulating behavior in ultrathin bismuth selenide field effect transistors.** *Nano Letters* 2011, **11**(5):1925–1927.
22. Wu S, Liu G, Li P, Liu H, Xu H: **A high-sensitive and fast-fabricated glucose biosensor based on Prussian blue/topological insulator Bi2Se3 hybrid film.** *Biosens Bioelectron* 2012, **38**(1):289–294.
23. Mellnik A, Grab J, Mintun P, Lee JS, Richardella A, Samarth N, Ralph D: **Efficient generation of spin current and spin transfer torque by the topological insulator bismuth selenide.** *Bull Am Phys Soc* 2013, **58**:00011.
24. Hong SS, Cha JJ, Kong D, Cui Y: **Ultra-low carrier concentration and surface-dominant transport in antimony-doped Bi2Se3 topological insulator nanoribbons.** *Nat Commun* 2012, **3**:757.
25. Choi YH, Jo NH, Lee KJ, Yoon JB, You CY, Jung MH: **Transport and magnetic properties of Cr, Fe, Cu-doped topological insulators.** *J Appl Phys* 2011, **109**:07E312.
26. Alemi A, Hanifehpour Y, Joo SW, Min BK, Oh TH: **Structural studies and optical and electrical properties of novel Gd^{3+}-doped Sb2Se3 nanorods.** *J Nanomater* 2012, **2012**:70.
27. Song L, Zhang S, Chen C, Hu X, Wei Q: **Synthesis of sulphur doped bismuth selenide photocatalysts by the solvothermal method and their photocatalytic activities under visible-light irradiation.** *Chem Eng J* 2011, **171**(3):1454–1457.
28. Kandala A, Richardella A, Zhang D, Flanagan TC, Samarth N: **Surface-sensitive two-dimensional magneto-fingerprint in mesoscopic Bi2Se3 channels.** *Nano Letters* 2013, **13**(6):2471–2476.
29. Lei J, Qie N, Zhou J, Hua Y, Ji T: **Preparation and characterization of TiO2 nanobelts deposited with Bi2Se3 nanoplates.** *Mater Lett* 2012, **83**:108–111.
30. Yu CL, Yang K, Shu Q, Yu JC, Cao FF, Li X, Zhou XC: **Preparation, characterization and photocatalytic performance of Mo-doped ZnO photocatalysts.** *Sci China Chem* 2012, **55**(9):1802–1810.
31. Wang X, Bai H, Meng Y, Zhao Y, Tang C, Gao Y: **Synthesis and optical properties of Bi^{3+} doped NaTaO3 nano-size photocatalysts.** *J Nanosci Nanotechnol* 2010, **10**(3):1788–1793.